JACS
JOURNAL OF THE AMERICAN CHEMICAL SOCIETY

Article

pubs.acs.org/JACS

Ionic Strength Modulation of the Free Energy Landscape of Aβ_{40} Peptide Fibril Formation

Axel Abelein,[†,§] Jüri Jarvet,[†,‡] Andreas Barth,[†] Astrid Gräslund,[†] and Jens Danielsson*[,†]

[†]Department of Biochemistry and Biophysics, Stockholm University, Svante Arrhenius väg 16, SE-106 91 Stockholm, Sweden
[‡]The National Institute of Chemical Physics and Biophysics, Akadeemia tee 23, 12618 Tallinn, Estonia

Supporting Information

ABSTRACT: Protein misfolding and formation of cross-β structured amyloid fibrils are linked to many neurodegenerative disorders. Although recently developed quantitative approaches have started to reveal the molecular nature of self-assembly and fibril formation of proteins and peptides, it is yet unclear how these self-organization events are precisely modulated by microenvironmental factors, which are known to strongly affect the macroscopic aggregation properties. Here, we characterize the explicit effect of ionic strength on the microscopic aggregation rates of amyloid β peptide (Aβ40) self-association, implicated in Alzheimer's disease. We found that physiological ionic strength accelerates Aβ40 aggregation kinetics by promoting surface-catalyzed secondary nucleation reactions. This promoted catalytic effect can be assigned to shielding of electrostatic repulsion between monomers on the fibril surface or between the fibril surface itself and monomeric peptides. Furthermore, we observe the formation of two different β-structured states with similar but distinct spectroscopic features, which can be assigned to an off-pathway immature state (F_β*) and a mature stable state (F_β), where salt favors formation of the F_β fibril morphology. Addition of salt to preformed F_β* accelerates transition to F_β, underlining the dynamic nature of Aβ40 fibrils in solution. On the basis of these results we suggest a model where salt decreases the free-energy barrier for Aβ40 folding to the F_β state, favoring the buildup of the mature fibril morphology while omitting competing, energetically less favorable structural states.

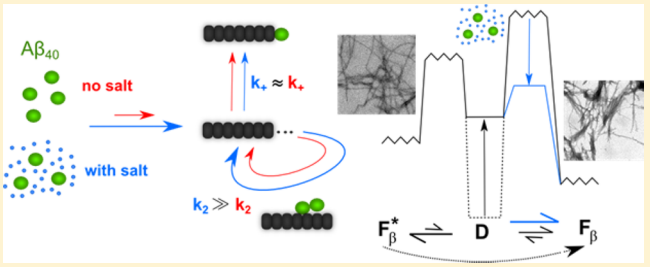

INTRODUCTION

Self-assembly and aggregation of proteins and peptides into insoluble fibrillar aggregates is closely associated with pathogenesis of neurodegenerative diseases, and among them the most prevalent example, Alzheimer's disease (AD).[1,2] The appearance of amyloid plaques in patients' brains is one hallmark of this disease.[3] The major components of these aggregates are β-sheet rich fibrils where a major component is a small peptide, most frequently 40 or 42 residues long, the amyloid β peptide (Aβ40 and Aβ42).[3] Identifying and controlling the pathways of aggregation have been challenging, yet is the key for a detailed understanding of the molecular mechanisms underlying peptide and protein aggregation in neurodegenerative diseases.[2] Different molecular events contribute to the generation of new aggregates and can be classified into primary and secondary nucleation reactions in addition to fibril-end elongation.[2,4] Several reports have demonstrated that formation and structural properties of amyloid fibrils are highly dependent on environmental conditions, such as peptide or protein concentration, temperature, pH, the presence of metal ions and ionic strength (reviewed in ref 5). Elucidation of the link between these factors and modulation of aggregation behavior is essential to obtain comprehensive knowledge about the pathways and causes of protein/peptide misfolding. To clearly pinpoint the effect of individual environmental factors on fibril formation, detailed kinetic and structural studies in vitro have to be performed. This kind of benchmarking is essential in order to understand and mimic physiological conditions. The relatively high ionic strength found in vivo, which mainly originates from the high concentration of sodium, potassium and chloride ions as well as charged biomolecules, has been shown to affect protein/peptide folding pathways by modulation of the electrostatic interactions.[6,7] Besides a modulation effect on aggregation kinetics due to electrostatic influences, it has been reported that final Aβ fibrils exhibit morphological differences depending on the ionic strength.[7] In the present study, we investigate, in detail, the effect of sodium salts, at physiological concentrations, on the molecular mechanism of aggregation of Aβ40 (i.e., the predominant and less aggregation prone peptide variant) and the accompanying structural changes of the peptide during the entire aggregation process. This aggregation process is governed by a set of microscopic rate constants, and from a detailed analysis of the aggregation kinetics, we pinpoint which rate constant is predominantly affected by an increase in ionic strength. We demonstrate that also the fibril morphology is affected by the salt concentration in which they are formed. Furthermore,

Received: May 2, 2016
Published: May 12, 2016

DOI: 10.1021/jacs.6b04511
J. Am. Chem. Soc. 2016, 138, 6893−6902

fibrils already formed at low ionic strength undergo a morphological transition when salt is added, underlining the dynamic properties of Aβ40 fibrils in aqueous solution. The different fibril morphologies are spectroscopically characterized, and we show that although both fibril types are built up by a β-sheet structure, they differ in the specific structural arrangement.

MATERIALS AND METHODS

Sample Preparation. The 40 residue long amyloid β peptide recombinant variant Aβ40 was purchased from Alexo-Tech (Umeå, Sweden) and samples were prepared as described previously[8,9] by dissolving the peptide in 10 mM NaOH to 1−2 mg/mL and subsequent dilution in sodium-phosphate buffer. For Thioflavin T (ThT) fluorescence kinetics 0.02% NaN_3 and 40 μM ThT were added to the sample and a 10 mM buffer concentration, pH 7.2, was used. The circular dichroism (CD) experiments were conducted with 10 μM Aβ40 in 2 or 5 mM buffer, pH 7.2, or 200 μM Aβ40 prepared in a D_2O solution, which was adjusted by small amounts of NaH_2PO_4 to pH 7.0 (measured in D_2O, value from pH meter reading) for combined CD-FTIR (Fourier transformed infrared) studies.

NMR Spectroscopy. ^{1}H-{^{15}N} heteronuclear single quantum spectra (HSQC) were acquired on a 700 MHz Bruker Advance spectrometer (equipped with a cryo-probe) at 8 °C on 80 μM Aβ40 in 10 mM sodium-phosphate buffer, pH 7.3. After salt titration with 50, 100, and 150 mM NaF the peptide concentration was diluted to 68 μM. Transversal relaxation, R_2, was determined by a standard ^{1}H-{^{15}N}HSQC based experiment with 8 delays, 10, 30, 50, 80, 100, 150, 200, and 250 ms. 50 and 150 ms were measured twice in order to estimate experimental precision.

ThT Fluorescence Kinetics. ThT fluorescence experiments were conducted on a Fluostar Omega (BMG Labtech) fluorimeter using a 96 well plate. ThT signals, excitation wavelength 440 nm and emission at 482 nm, were recorded at 37 °C under quiescent conditions with a time interval of 3 min between recordings. Aggregation traces were fitted using a sigmoidal function $F = F_0 + 1/(1 + \exp[r_{max}(\tau_{1/2} - t)])$, where $\tau_{1/2}$ is the time for half completion of aggregation and r_{max} is the maximum growth rate. Aggregation half times $\tau_{1/2}$ showed a dependence on the initial monomer concentration, $m(0)^{\gamma}$, which can be described by a power law $\tau_{1/2} \propto m(0)^{\gamma}$, where the half time exponent γ is related to the nucleation process.[4,10] For global fit analysis aggregation curves were normalized and averaged, in general, over 5 replicates (neglecting a few apparent outliers that exhibit a very different shape of the aggregation trace). Kinetic traces at different NaF concentrations were variance weighted before averaging. Averaged and normalized data were fitted with an aggregation model proposed by Meisl et al.[11] The model and fitting routine are described in detail in ref 9. Seeds for seeding experiments were obtained from aggregated samples from previous experiments under exactly the same conditions. For experiments with different seed concentrations, seeds were obtained from a 20 μM aggregated sample. For estimation of the elongation rate, monomeric peptide and seeds were mixed in the ThT plate to a final ratio of 10 μM monomers to 10 μM seeds. Aggregation traces were normalized, and initial slopes were determined from linear fits to the time points of the first 78 min.

Circular Dichroism. CD spectra in the far-UV region (250−190 nm) were recorded with a Chirascan CD spectrometer (Applied Photophysics, Leatherhead, U.K.) equipped with a Peltier temperature control unit. Aggregation kinetics for 10 μM peptide was detected in a 4 × 10 mm CD quarz cuvette at 37 °C and using a bandwidth of 1 nm, a step size of 1 nm with 1.5 s accumulation time per point in time steps of 3 min. To monitor CD aggregation kinetics within a feasible time frame the samples were continuously stirred during the entire measurement by a small magnet, in contrast to the ThT kinetics that was recorded under quiescent conditions. We found that under continuous stirring the CD spectra for Aβ40 featured a very similar pattern as under quiescent conditions (Supporting Information).

Combined Circular Dichroism and Infrared Experiments. For combined CD and FTIR studies a 200 μM Aβ40 sample in D_2O solution was used. The sample was incubated analogously as for CD kinetics experiments at 37 °C in a 4 × 10 mm quarz cuvette under continuous stirring. Measurements were performed at 20 °C on small aliquots (3 μL) transferred to a CaF_2 cuvette with an optical path length of 50 μm, which is both applicable for CD and FTIR experiments. CD signals were acquired using a bandwidth of 1 nm, 0.5 s-per-point, step size of 0.5 nm and signals averaged over 10 scans.

FTIR measurements were conducted subsequently on exactly the same sample with the same cuvette on a Bruker Tensor 37 spectrometer (Bruker Optics, Germany). Interferograms were acquired at 20 °C at 4 cm^{-1} resolution, Fourier-transformed with a zero-filling factor of 2 and averaged over 26 scans.

Calculation of Theoretical CD Spectra. CD spectra of Aβ structures deposited in the protein data bank (PDB) were used for calculations using the program *DichroCalc*,[12] including backbone charge-transfer and side chain transitions.

Transmission Electron Microscopy (TEM). TEM grids were prepared from aggregated Aβ40 samples incubated without 150 mM NaF and from Aβ40 aggregates initially prepared without salt that were further incubated in the presence of 150 mM NaF (same conditions as used for CD and FTIR experiments) that exhibited CD minima at approximately 216−217 and 222 nm, respectively. Carbon-coated 200-mesh copper grids were placed on top of 15 μL sample droplets, blotted for ca. 10 min and stained with 1% uranyl acetate. TEM images were recorded on a Tecnai G2 Spirit BioTWIN microscope with a tungsten filament operating at 80 kV.

Dynamic Light Scattering (DLS). DLS measurements were performed on aggregated Aβ40 samples as used for CD measurements, exhibiting CD minima at 215 and 222 nm. An ALV/CGS-3 compact goniometer system (ALV-GmbH, Langen, Germany) with a HeNe laser (632.8 nm) was used, applying a scattering angle of 150°. Autocorrelation curves were measured over a period of 30 s and averaged over 20 runs.

RESULTS AND DISCUSSION

Salts Accelerate Aβ40 Fibril Formation. To investigate the effect of salt on Aβ40 aggregation we conducted ThT fluorescence and CD aggregation kinetics experiments with and without sodium chloride (NaCl) and fluoride (NaF). The time dependence of ThT fluorescence intensity upon Aβ aggregation, under quiescent conditions, can typically be approximated by a sigmoidal trace.[9,13] The sigmoidal trace is fully characterized by the aggregation half time $\tau_{1/2}$ and the maximum growth rate r_{max}. Assuming that the ThT fluorescence linearly reports on Aβ aggregation, we monitored the aggregation kinetics of 20 μM Aβ40, at physiological pH, in the presence and absence of NaCl. As expected, the aggregation traces of Aβ40 alone exhibit sigmoidal patterns (Figure 1). In

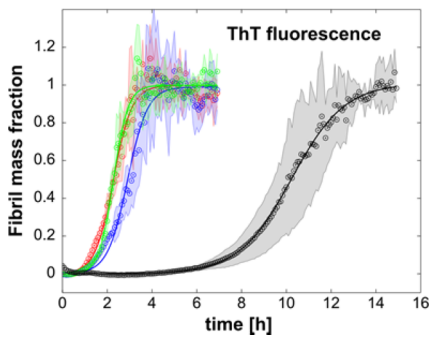

Figure 1. ThT fluorescence kinetic aggregation traces of 20 μM Aβ40 in the absence (black) and presence of 150 mM NaCl (blue), NaF (red) and LiCl (green). The shaded areas reflect the standard error bar from five replicates, underlining that the variability in aggregation kinetics scales with the lag time.[14,15]

DOI: 10.1021/jacs.6b04511
J. Am. Chem. Soc. 2016, 138, 6893−6902

the presence of 150 mM sodium salt the aggregation kinetics is strongly accelerated (Figure 1). To test if this effect is directly linked to the identity of the salt ions we determined the aggregation kinetics also in the presence of NaF and LiCl. Indeed, the effect of sodium ions with either chloride or fluoride as anions on the aggregation traces is very similar (Figure 1) and the aggregation half time for 20 μM Aβ40 decreases from 10.3 ± 1.1 h for Aβ40 alone to 3.0 ± 0.3 h and 2.3 ± 0.1 h for 150 mM NaCl and NaF, respectively. Similarly, changing the cation Na^+ to Li^+ causes a very similar acceleration of fibril formation as the corresponding sodium salts (Figure 1), yielding a $\tau_{1/2}$ value of 2.3 ± 0.1 h in the presence of 150 mM LiCl.

An Increased Ionic Strength Does Not Change the Concentration Dependence of Aβ40 Aggregation. To obtain insight in how increased ionic strength accelerates Aβ40 aggregation kinetics we performed a detailed analysis of the peptide concentration dependence for fibril formation. To quantitatively analyze Aβ aggregation we used the framework proposed by Knowles et al.[4,10,11,16] where the growth of fibril mass is dependent on (i) the number of free ends acting as growth sites and (ii) fibril elongation. The number of free ends increases by formation of primary nuclei, but also by secondary pathways. Primary nucleation is the formation of an aggregate by monomers which is competent to template further fibril formation, and is characterized by the formation rate k_n and the size of the nucleus, n_c. Secondary pathways for formation of new fibril ends include breakage of existing fibrils characterized by the fragmentation rate, k_-, and monomer-dependent secondary nucleation, i.e., monomer−monomer interactions catalyzed by the fibril surface, characterized by the rate k_2, and the reaction order n_2.[4,10,17] For simplicity, the microscopic rate constants are assumed to be well-defined and reporting on one single process each. For a complete description of the model, cf. refs 4 and 11. To elucidate how salt affects the aggregation mechanism we performed aggregation kinetics experiments under quiescent conditions at different peptide concentrations in the range of 10−20 μM Aβ40 in the absence and presence of 150 mM NaF (Figure 2A and B). Due to favorable properties of fluoride anions compared to chloride ions for subsequent structural studies using CD spectroscopy, the fluoride salt variant was chosen also for the ThT fluorescence kinetics studies. The aggregation half time, $\tau_{1/2}$, is peptide concentration dependent and the relationship can be described by a simple power law:

$$\tau_{1/2} \propto m(0)^{\gamma} \quad (1)$$

where $m(0)$ is the total monomer concentration and $\tau_{1/2}$ is the half time for aggregation completion. The exponent, γ is characteristic for the nucleation process and ranges from −0.5 for completely fragmentation-dominated processes to −1.5 for secondary processes that are dominated by monomer-dependent surface-catalyzed secondary nucleation events.[4,10] For Aβ40 the γ-value itself has been reported to be peptide concentration-dependent with values ranging from −1.2 at relatively low concentrations to −0.2 at very high concentrations where the secondary nucleation process is saturated.[11] Here, we found that Aβ40 alone, i.e., in the absence of high salt concentration, yields a half-time exponent of γ = −0.9 ± 0.1 (Figure 2C) in the concentration range of 10−20 μM, in excellent agreement with previous findings, and in accordance with a process dominated by surface catalyzed secondary nucleation.[9,11] Upon addition of 150 mM NaF the γ-value is slightly, but not

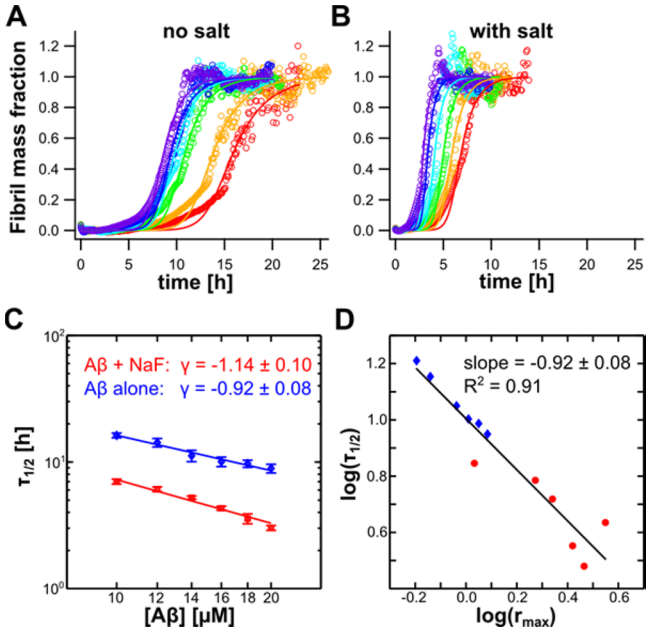

Figure 2. Aggregation kinetics of Aβ40 alone (A) and in the presence of 150 mM NaF (B) at different peptide concentrations with global fits of all aggregation traces for 10 (red), 12 (orange), 14 (green), 16 (cyan), 18 (blue) to 20 μM (violet) Aβ40. (C) Mean aggregation half times $\tau_{1/2}$ are dependent on the initial peptide concentration $m(0)$ described by the power law $\tau_{1/2} \propto m(0)^{\gamma}$ with a half time critical exponent γ. Aβ40 alone (blue) and in the presence of 150 NaF (red) exhibit similar γ-values. (D) The correlation plot of the logarithmic values of $\tau_{1/2}$ and the maximum growth rate r_{max} shows a slope of −0.9 ± 0.1. $\tau_{1/2}$ and r_{max} shown in (C) and (D) are determined from fitting an empirical sigmoidal equation to the aggregation traces.

significantly, higher with γ = −1.1 ± 0.1. Notably, under these conditions no significant curvature in $\gamma([A\beta40])$ is found. Furthermore, when plotting the aggregation half times versus the maximum growth rate on a double-logarithmic scale, the two data sets, i.e., with and without salt, fall on the same line with a slope of −0.9 ± 0.1. This is within experimental accuracy the expected slope of −1 for an aggregation process dominated by secondary processes (Figure 2D). It should be underlined that the observables measured by this method do not reveal any direct details on primary nucleation, which is present along all stages of the aggregation process. We conclude that the presence of 150 mM NaF considerably accelerates Aβ40 aggregation without changing the dominating mechanism, reported in the concentration dependence.

Changes in Microscopic Rate Constants in Salt Induced Acceleration of Aβ40 Aggregation from Global Fit Analysis. In order to determine the effect of NaF on the microscopic rates we performed an analysis where the aggregation traces from all peptide concentrations were fitted globally to an aggregation-nucleation model including saturation of secondary nucleation (k_2), which is described by a generalized Michaelis constant K_M. In this analysis the microscopic nucleation rates are fitted as combined parameters, i.e., the square root of the combined rate constants for primary, $\sqrt{k_n k_+}$, and secondary nucleation, $\sqrt{k_+ k_2}$, as well as saturation of secondary nucleation, K_M, are free fitting parameters. The results from these fits are listed in SI Table S1 and shown in Figure 2A and B. Although the model does not precisely capture the early stage aggregation behavior, the overall fit is

DOI: 10.1021/jacs.6b04511
J. Am. Chem. Soc. 2016, 138, 6893−6902

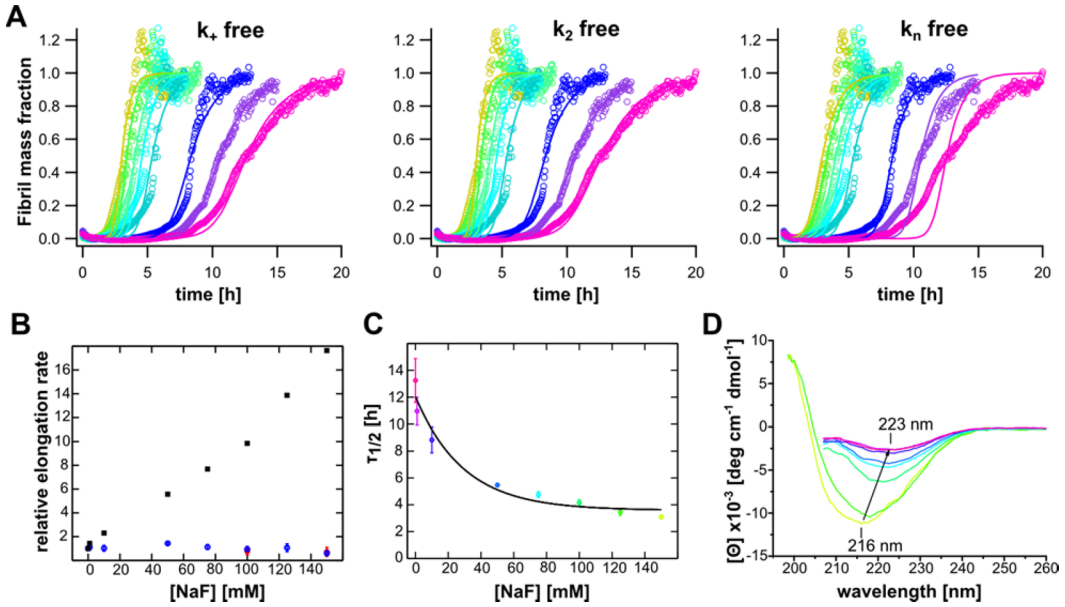

Figure 3. (A) Aggregation kinetics of 20 μM Aβ40 in the presence of different NaF concentrations ranging from 0 (pink) to 150 mM (yellow). In a global fit analysis the fitting parameters were constrained such that only one rate constant is the effective free fitting parameter and the others are fixed to the same value across all NaF concentrations. While k_n as the sole fitting parameter resulted in an insufficient fit (RSS = 15.5), both an exclusive change in either k_+ or k_2 reflected well the observed behavior with RSS values of 8.1 and 7.9, respectively. (B) Relative elongation rate determined from seeding experiments in the presence of different concentrations of NaF (blue circles) and NaCl (red diamonds) compared to the relative elongation rate determined from global fit analysis (black squares). (C) Mean $\tau_{1/2}$ values exhibit an exponential response on the NaF concentration given by $\tau_{1/2} = A\cdot\exp(-m\cdot[\mathrm{NaF}])\tau_\infty$ with m = 0.03 ± 0.01 mM^{-1}, A = 8.5 ± 0.7 h and τ_∞ = 3.6 ± 0.6 h. Error bars display the standard deviation from five replicates. (D) CD signals of ThT samples taken from the final plateau phase in (A) exhibit a shift of the CD minimum to longer wavelengths with increasing NaF concentration accompanied by a signal intensity loss.

good, especially in the maximum growth regime. In low salt solutions the fitted values are in agreement with earlier findings,[9] while notably, in 150 mM NaF solution both combined rate constants increase by a factor 2−3 and also the saturation constant K_M increases albeit afflicted with a relative large fitting error. The change in K_M indicates that particularly k_2 is influenced by the presence of salt.[9,11]

In order to further characterize which microscopic aggregation rate that is most affected by the presence of salt we performed aggregation experiments at constant peptide concentration (20 μM) and different NaF concentrations (0−150 mM) (Figure 3A). Following the procedure described above data could be fitted globally where one of k_n, k_+ or k_2 is allowed to vary for different salt concentrations while the others are fitted with one value for all conditions. This analysis shows that the overall global fit is significantly better when exclusively k_+ or k_2 is altered (RSS 7.9 and 8.1) compared to when k_n is fitted as the sole parameter (RSS 15.5). Looking into the fits in more detail reveals that at low salt concentration the fits with k_+ and k_2 as free parameters are significantly better than with k_n as free parameter, but at high salt concentration all fits are equally good (Figure 3A and SI Figure S1). This could be due to that both secondary and primary pathways for formation of new aggregates are accelerated by salt, and the salt dependence is stronger for primary nucleation making it the dominating mechanism for generation of new fibrils at high ionic strength. To test this hypothesis we examined how the dominating fibril mass growth mechanism is affected by salt.

It has previously been shown, by others and us, that Aβ40 fibril mass growth in the absence of salt is dominated by secondary nucleation under quiescent conditions.[9,11] To investigate whether this mechanism is also dominant in the presence of salt we conducted kinetic experiments where low concentrations of preformed seeds, i.e., aggregated Aβ40, were added to fresh monomeric Aβ40, under conditions where it is known that formation of primary aggregates are below the detection limit, i.e., during the so-called lag phase (SI Figure S2).[4] The free monomer concentration with and without seeds is the same so any significant initiation of growth by seeds within the lag time for a nonseeded sample is due to formation of new aggregates by secondary pathways. We find a rapid sigmoidal growth of fibril mass in the presence of seeds, and the plateau phase is reached within the lag phase of an unseeded sample. This demonstrates that also in the presence of salt the overall dominating mechanism for formation of new aggregates is governed by secondary nucleation events.[4]

This analysis suggests that a change in the primary nucleation rate, k_n, cannot sufficiently explain the salt effects (Figure 3A and SI Figure S1), especially not under the full span of salt concentrations studied here. Indeed, the primary nucleation rate is most likely accelerated by salt, but as the fibril mass growth is completely dominated by secondary pathways, also at high salt concentration, all such effects are effectively obscured. This finding is also underlined by the reasoning that changing k_n alone cannot account for the observed correlation between r_{max} and $\tau_{1/2}$ (Figure 2D and 3A). Changing exclusively k_+ or k_2, on the other hand, better accounts for the observed salt effects over the full concentration interval (Figures 3A, 3B and SI Figure S1 and S3A). The global fit analysis, however, lacks detailed information about which of these rate constants that is predominately enhanced even though the increase in K_M upon addition of salt indicates that k_2 should be affected (SI Table S1).

DOI: 10.1021/jacs.6b04511
J. Am. Chem. Soc. 2016, 138, 6893−6902

Thus, to identify whether k_+ or k_2 is the primarily affected parameter by salt we conducted additional aggregation experiments in the presence of high concentration of preformed seeds, i.e., aggregated Aβ40. Under highly preseeded conditions, corresponding to the late-stage kinetic profile (above the inflection point), monomers are greatly depleted, and in this regime the concave kinetic trace is dominated by the process with the weakest dependence on the monomer concentration,[4] i.e., the elongation rate in the case of Aβ40. We used seeds prepared from 10 μM aggregated Aβ40 and added 10 μM fresh monomers, which resulted in concave aggregation traces where the initial linear slope was determined (SI Figure S3B). Interestingly, we found that this initial slope is basically unaffected by addition of salt (Figure 3B and SI Figure S3B), i.e., the elongation rate appears to be constant and independent of salt, albeit this kind of experiments is typically affiliated with a large variance due to the heterogeneity of seeds. This then falsifies the hypothesis that k_+ is the main affected microscopic rate constant, which could not be resolved from the global fit analysis alone (see above and Figure 3A). Together, these findings suggest hence that the drastic change in aggregation kinetics observed upon addition of sodium salt predominantly is caused by an increase in secondary nucleation rate, while potential masked effects on k_+ and k_n play a minor role.

Salt Concentration Dependent Effect on Aβ40 Aggregation. Salt may affect fibril formation in more than one way, e.g., specific binding, electrostatic screening, and Hofmeister effects.[18,19] Electrostatic screening should be similar for all ions of the same valence, while direct binding and Hofmeister effects should show ion specificity. In addition, these mechanisms are present at different ion concentrations: specific binding can occur already at low concentration, while Hofmeister effects extend 1 M ionic strength and above.[20] Electrostatic screening on the other hand typically is important at concentrations where the Debye length is between 5 and 20 Å, corresponding to 0.02−0.3 M ionic strength.[21,22] To obtain some information on the nature of the salt effect we quantified the effect of NaF on the aggregation kinetics (Figure 3A) and found strong salt concentration dependence where the aggregation half time exhibits an exponential response that can be described by

$$\tau_{1/2} = A\cdot\exp(-m\cdot[\mathrm{NaF}]) + \tau_\infty \quad (2)$$

with the parameters m = 0.03 ± 0.01 mM^{-1}, A = 8.5 ± 0.7 h and τ_∞ = 3.6 ± 0.6 h (Figure 3C). The generalized linkage coefficient, m, is defined by the electrostatic architecture of the system.[22] Interestingly, $\tau_{1/2}$ does not extrapolate to zero as [NaF] goes toward infinity but levels off at 3.6 h. This suggests out that the effects measured here are not Hofmeister effects and indicates that salt screens electrostatic interactions. The screening effect levels out at approximately 150 mM NaF where the Debye length is about 8 Å.[23] These findings suggest that the increased secondary nucleation rate stems from shielding of electrostatic repulsion.

Sodium Salt Does Not Bind Specifically to Monomeric Aβ40. Although archetypical screening effects are found in the salt-concentration dependence, we cannot rule out that also specific monomeric ion interactions occur which also may affect the aggregation kinetics. It has previously been shown, by others and us, that Aβ40 specifically binds divalent metal ions such as copper and zinc and that this effectively modulates the aggregation kinetics on the level of secondary aggregation pathways.[9,24,25] To investigate whether such specific monomer binding takes part in salt modulation of Aβ40 aggregation we recorded a series of ^{1}H-{^{15}N}-heteronuclear single quantum spectra (HSQC) with 0, 50, 100, and 150 mM NaF. In line with previous findings[26] we found only minute chemical shift changes upon addition of salt, (SI Figure S4A). The most affected cross-peaks correspond to residues close to the His, Asp, Glu, Arg and Lys side chains, (SI Figure S4B−C). These small chemical shift changes may be due to screening of transient electrostatic interactions and/or salt dependent shifts in pK_a values.[22] Furthermore, no sequence dependent change in relative intensity was found (SI Figure S4D), indicating that no significant specific ion binding occurs on an intermediate exchange rate. We conclude that specific ion binding to Aβ40 monomer does not contribute to the observed increase in aggregation kinetics.

The chemical shift perturbation by salt is overall very small. Nevertheless, some systematic chemical shift can be identified, especially in the ^{15}N dimension, where the C-terminal hydrophobic stretch (residues 31−40) of Aβ40 apparently is systematically shifted (SI Figure S4C). This may be due to a change in the structural ensemble of the intrinsically disordered Aβ40 as a consequence from the charge screening. An increase in structural propensity has been shown to facilitate binding and folding,[27] and may indeed also influence Aβ40 self-assembly, both in terms of primary nuclei formation and secondary nucleation. To quantify the effect on structural preferences we determined the secondary structure propensity from NMR chemical shifts[28] and found that the effect of salt is, again, very small. Interestingly the sign of the induced shift changes suggest a 0.6% decrease of β-propensity in the C-terminal hydrophobic segment, typically assigned to be part of the fibril backbone (SI Figure S4E). Residual structure and binding show typically a relatively weak positive correlation,[29] and the found decrease in transient structure is not likely to account for the observed increase in aggregation kinetics. Conversely, in a recent report Aβ40 and Aβ42 have been shown to show very similar residual structure, while they exhibit significantly different aggregation properties.[26]

To obtain more insight into residual structure and potential intermolecular exchange dynamics we measured the ^{15}N transverse relaxation rate, R_2, and found a general increase in R_2 for all residues with ΔR_2 = 2.05 ± 0.85 s^{-1} (SI Figure 4F). In general, chemical exchange between different states causes an increase in R_2 and Aβ40 has been shown to undergo exchange between free monomers and a state where it is bound to an NMR invisible aggregate.[30,31] This exchange process is manifested as a general increased R_2 relaxation rate due to the very fast relaxation of the large proto-fibrillar structures, where the increase in R_2 exhibits a similar value as in our system. Presuming such an exchange system, salt ions may screen the repulsion between Aβ40 monomers and the fibril surface and thereby increase the bound population.

Taken together the data suggest that sodium fluoride does not specifically bind to Aβ40 and the surface catalyzed formation of new fibrils is accelerated by salt via electrostatic shielding of, most likely, both repulsion between monomers on the fibril surface and between the surface itself and monomers in surrounding solvent. This is in line with previous findings where the reduction of electrostatic repulsion by replacing charged amino acid by neutral side chains effectively reduced aggregation rates.[15]

DOI: 10.1021/jacs.6b04511
J. Am. Chem. Soc. 2016, 138, 6893−6902

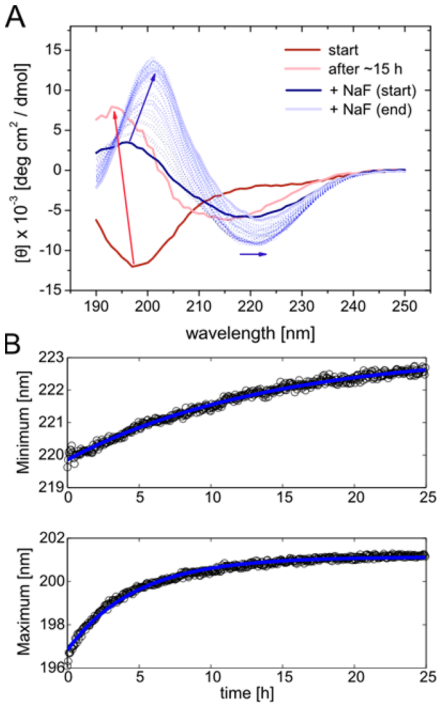

Figure 4. (A) CD aggregation kinetics of 10 μM Aβ40. After ~15 h incubation without salt (red), 150 mM NaF was added that caused a slow structural transition (from dark to light blue) from F_β* to F_β. (B) The time dependence of spectral peaks exhibits an exponential dependence with half-times of 14.2 ± 0.3 h and 4.8 ± 0.1 h for the CD minimum and maximum, respectively.

High Ionic Strength Favors a Morphologically Mature Fibrillar State. The question is now how the fibrillar structure and morphology are affected by a high ionic strength. CD spectroscopy is a low-resolution method that allows the direct observation of secondary structure changes during the aggregation process in the absence and presence of sodium salt. We observed differences in the CD spectra of aggregated Aβ40 depending on salt concentration (Figure 3D). Without added salt the CD spectrum indicated a β-structure with a spectral minimum at 216 nm, which we refer to as F_β*. With increasing NaF concentration, the overall spectral features are still consistent with a β-structure, but the position of the minimum shifts to longer wavelengths up to 223 nm at the highest salt concentration (150 mM NaF), and we assign this morphological state to F_β. The shift of the minimum is accompanied by a reduction in CD signal intensity, which may be due to increased scattering (Supporting Information). Thus, a change in the morphology of the fibrils is observed, and we conclude that the presence of salt favors one of the structural states.

In order to characterize the formation of these β-structures in more detail we followed the time dependence of the structural changes from an initial random coil-like structure to the final β-structures F_β* and F_β (Figures 4A, 5A and SI Figure S5). The aggregated state F_β* is characterized by a maximum at around 193 nm and a minimum at around 216 nm. Without salt the structural conversion to F_β* occurred within a few hours and remained, apart from some signal loss, constant for many hours (monitored for up to 1 day). Interestingly, no isodichroic point(s) (SI Figure S5A) is/are present in the CD spectra,

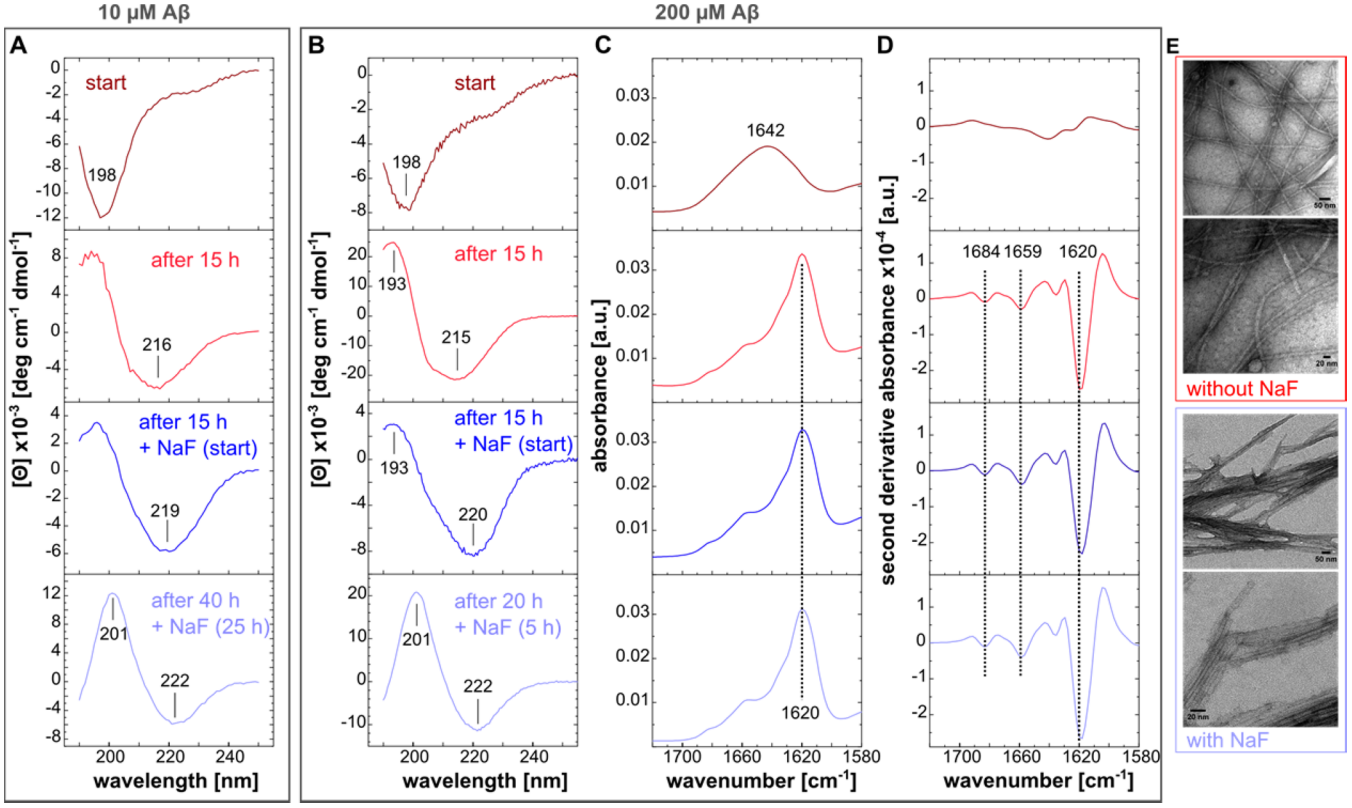

Figure 5. (A) CD measurements on 10 μM Aβ40 at different time points without (red) and after addition of 150 mM NaF (blue) showing the far-UV CD spectrum. (B–D) Combined CD and FTIR measurements on 200 μM Aβ40 where the CD (B), FTIR absorbance (C) and second derivative (D) are shown. (E) TEM images without NaF (corresponding to the state after 15 h) and after addition and incubation with NaF for 5 h.

DOI: 10.1021/jacs.6b04511
J. Am. Chem. Soc. 2016, 138, 6893–6902

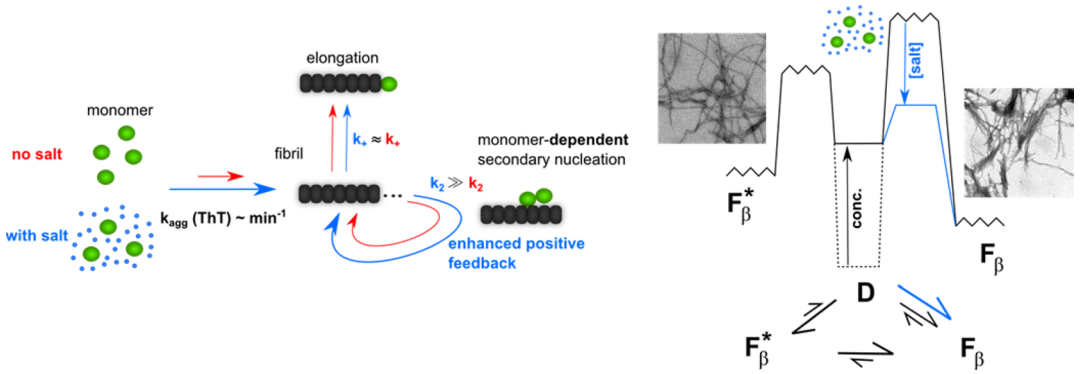

Figure 6. Aβ40 fibril formation is dominated by a secondary nucleation mechanism where an increase ionic strength highly accelerates monomer-dependent secondary nucleation events by electronic shielding of repulsive charges on the fibril surface and monomers. In a schematic model, two distinct states, F_β* and F_β, with different structural morphology are present in Aβ40 aggregation where the presence of salt promotes the formation of an energetically favored β-structured state F_β by lowering the energy barrier toward this state.

suggesting that aggregation is not a simple two-state process. In agreement with the results of the ThT-detected aggregation experiments the presence of 150 mM NaF substantially accelerated the conformational change from random coil-like to mainly β-structure (SI Figure S6A). Again, compared to aggregation in the absence of salt the positions of the characteristic spectral extrema shift to longer wavelengths, i.e., from ~216 nm to ~222 nm and ~193 nm to ~200 nm for the spectral minimum and maximum, respectively (Figures 4A, 5A and SI Figure S6B)

Notably, also an Aβ40 sample in the absence of salt that had been incubated for a time period of about 4 days eventually displayed a similar CD spectrum as with salt where in particular the 216 nm spectral shift to longer wavelengths is evident (SI Figure S6B). Taken together, these findings suggests that F_β does not seem to be a state occurring exclusively in the presence of salt but may be assigned to the mature, low energy state in a conversion of immature to mature fibrils, and that the rate of maturation is salt concentration dependent (Figure 6).

Conversion between F_β* and F_β Is Slow. Subsequently, we asked ourselves whether F_β* is an immature state on pathway to the mature F_β? If so, addition of salt to preformed F_β* should induce a conversion to mature F_β, on a time scale faster than overall aggregation. Indeed, we found that such structural conversion is triggered by addition of 150 mM NaF to a F_β* sample initially aggregated in the absence of salt (Figure 4). However, after a fast initial burst phase this occurs on a very slow time scale. The conversion rate constant k_c is $\log(k_c/s^{-1}) = -4.45 \pm 0.25$ at 37 °C (Figure 4B), which is very slow compared to the much faster conformational change from random coil to F_β, under aggregation in the presence of salt, which takes place with $\log(k_{agg}/s^{-1}) \approx -3.2$ (SI Figure S5). In fact, the conversion rate is slower than the typical off rate of monomers from fibrils.[32−34] Kinetically, this indicates that F_β* is not on pathway to F_β formation, but suggests that Aβ40 may unfold from F_β* in order to form F_β (Figure 6).

Combined CD and FTIR Measurements Reveal Complementary Structural Information. To shed more light on the structural properties of the structural states observed by CD, we applied an approach using both CD and FTIR spectroscopy to monitor the structural states during the aggregation process. In the FTIR experiments a much higher peptide concentration, here 200 μM Aβ40, has to be used and experiments were performed in D_2O. The experimental setup was designed such that FTIR and CD signals could be recorded on exactly the same sample. Reassuringly, even at such high Aβ40 concentration we found a very similar secondary structure transition to those observed at 10 μM peptide concentration, although faster, and addition of 150 mM NaF again accelerates the structural transition from preformed F_β* to F_β (Figure 5B). Taken together, also under conditions favorable for FTIR experiments the aggregation states show analog structural features as monitored by CD spectroscopy.

FTIR signals were measured in the liquid phase, avoiding preparation of dried peptide films, which is often used in combination with total reflectance FTIR spectroscopy. In agreement with CD measurements the FTIR spectra revealed a structural conversion from a predominantly unstructured state, which is characterized by the broad absorption band at 1642 cm^{-1}, to a β-structured state with a pronounced sharp absorption band at 1620 cm^{-1} (Figure 5C and 5D). Two further bands at 1659 and 1684 cm^{-1} are clearly visible in the second derivative of the absorbance, where the first originates from turns, while the latter is an additional β-structure feature.[35] The high wavenumber component at 1684 cm^{-1} is typically seen for antiparallel β-structures, whereas for parallel β-structures this band is either weak or not observable.[35] Although the presence of the 1684 cm^{-1} band is evident, its relatively low intensity indicates parallel β-structures. Most remarkably and in contrast to the findings using CD spectroscopy, F_β* and F_β exhibit basically identical FTIR spectra, suggesting that both states are very similar in terms of secondary structure and further structural details like hydrogen bonding strength and the relative orientation of adjacent β-strands (discussed further in Supporting Information). These findings underline that CD and FTIR techniques are sensitive to different morphological features of the β-structured aggregates and thus reveal complementary structural information.

Simple Structural Modeling of F_β* and F_β. The different CD spectra of the two β-structures, F_β* and F_β, may stem from a different structural origin, and amyloid is indeed generally a heterogeneous structural state. Published structures of amyloid forming peptides show diverse β-structure characteristics such as antiparallel or parallel β-sheet alignments, different twist angle between β-sheets, number of strands, etc.[36−41] In a recent report Micsonai et al. demonstrated the large impact of different β-structure arrangements on the CD spectrum.[42] Furthermore, theoretical calculations by Manning and Woody pointed out that the intersheet angle strongly influences the

DOI: 10.1021/jacs.6b04511
J. Am. Chem. Soc. 2016, 138, 6893−6902

CD characteristics.[43] These authors showed that an intersheet angle change from 0° to 45° causes a shift to longer wavelengths of both the β-structure characteristic CD peaks. We calculated theoretical CD spectra of different amyloid structures deposited in the protein data bank using the program *DichroCalc*.[12] We found that fibril structures of Aβ40 and Aβ42 deposited in PDB,[36,37,39] which were obtained after very long incubation time or in the presence of 150 mM sodium salt, exhibit a CD minimum around 222 nm (SI Figure S7), similar to the spectra we obtained under comparable conditions. Interestingly, both an artificially induced twist in the β-sheet alignment and within the β-strands causes a shift of the CD minimum to shorter wavelengths, in particular for shorter fibrillar structures, and a large change of the 190−200 nm band (SI Figure S8) leading to spectra resembling the CD spectrum of F_β*. Thus, different fibril twists of F_β* and F_β are a putative source for the spectral observations. These simple models contain no information on the detailed local structures, and consequently no relevant IR spectrum can be reconstructed from these models. Yet, besides different twists in the fibril arrangement also other structural features such as changes in the quaternary structure, which are not included in these simplified calculations, may contribute. Hence, we concluded from this reasoning that different changes in morphologies of F_β* and F_β could cause the observed spectral characteristics.

Visualization of Aggregates by Transmission Electron Microscopy Images. To characterize the morphological differences between F_β* and F_β we visualized the aggregates using transmission electron microscopy (TEM). The TEM-images revealed seemingly different fibril structures and arrangements for aggregates prepared without salt and aggregates initially prepared without salt that were further incubated in the presence of 150 mM NaF (Figure 5E and SI Figure 9A,B). Without NaF the fibrils show a pattern where the fibrils exhibit no apparent order relative to each other. Some fibrils are twisted, which is here characterized by the presence of adjacent crossovers, i.e., periodic points between turns in the overall fibril structure.[44] In contrast, after further incubation with NaF the TEM images show larger aggregates with an arrangement where fibrils are aligned with respect to each other and associate into flat, rather untwisted, supersheets. A previous comprehensive TEM analysis of Aβ40 fibrils with and without 500 mM NaCl by Klement et al.[7] showed that the average fibril width is slightly smaller in the presence of salt compared to without salt (16 ± 4 and 21 ± 3 nm, respectively) and a much larger fraction of fibrils (57%) does not exhibit any twist compared to Aβ40 alone (24%). It is, however, apparent that Aβ40 fibrils exhibit a large morphological diversity even within the same sample and the distribution of structures is highly dependent on experimental conditions.[7,44−46]

To test if the presence of larger superstructures is really reporting on a property of the F_β state rather than a specific salt effect we visualized aggregates that had, by time, equilibrated to the low energy F_β state at low salt concentration. Indeed, the fibrils show a remarkable similarity with fibrils prepared at high salt concentration (SI Figure S9C). This indicates that the observed change in CD spectra upon maturation from F_β* to F_β is either directly or indirectly linked to formation of these superstructures, which could be described as fibril bundles. The formation of quaternary superstructures should also be reflected in a change in size distribution of the aggregates, and indeed, dynamic light scattering shows a significant increase in aggregate size in the presence of 150 mM salt (SI Figure S10).

The results from the TEM analyses, presented here and found in literature, support thus the conclusion that Aβ40 can fold into two morphologically distinct amyloid structures where the differences in the CD signal may arise from variations in overall quaternary structure. This might also cause changes in the fibrils on the tertiary structure level, e.g., the degree of twisting, upon quaternary fibril assemble, while the molecular architecture at close distances is kept intact, as revealed by FTIR spectroscopy. Apparently, the presence of salt lowers the barrier for folding into the more stable Aβ40 amyloid morphology featuring larger superstructures.

■ CONCLUDING REMARKS

In vitro folding of Aβ40 into amyloid fibrils occurs on a seemingly very frustrated free energy landscape.[47] Small alterations in experimental conditions modulate not only the kinetics but also the population of different morphological states, which is determined by the microenvironment. Aβ40 can fold into at least two morphologically distinct fibrillar structures and salt lowers the barrier to the more stable structure, F_β, in vitro (Figure 6). The finding of such multiple morphologies of fibers from the same peptide sequence is in stark contrast from what is expected for folding of globular proteins, where typically the native state is very well-defined.[48,49] However, the small, but significant differences in fiber structures reported both from in vitro[37,46,50,51] and in vivo aggregates[52] underlines the structural diversity. The heterogeneity in the end-state fibril structures suggests that the structural ensembles along the aggregation pathway are also heterogeneous entities.[53] A detailed quantitative analysis depends on that ThT linearly reports on fibril formation as well as that the model combines multistep aggregation processes into interpretable rate constants. Reassuringly, Aβ aggregation shows the same kinetics when determined by CD or ThT fluorescence.[11] In summary, our findings can be rationalized in an aggregation model that characterizes the effect of sodium salt on the aggregation mechanism of Aβ40. In this model two processes are directly affected by ionic strength effects. From the ThT kinetic analysis we conclude that the general nucleation mechanism of Aβ40 aggregation is basically the same, yet the aggregation kinetics is greatly accelerated. This predominantly originates from an enhancement of the secondary nucleation rate k_2, while fibril-end elongation rate k_+ does not contribute significantly to the observed acceleration of fibril formation. The small increase, although within the error margins, in the monomer concentration dependence of Aβ40 aggregation, where $|\gamma|$ increases from 0.92 to 1.14 (Figure 2C), indicates that the level of saturation of k_2 is reduced by the faster secondary nucleation turnover rate, which includes formation and subsequent release of new aggregates from the fibril surface. The ThT analysis is not able to directly measure any effect on the primary nucleation rate k_n. However, the very strong effect by seeding seen both with and without salt show that the primary nucleation has a limited impact on the formation of new aggregates under the fast growth phase. Formation of fibrillar mass is under these conditions dominated by secondary aggregation mechanisms.

The general aggregation promoting effect of different sodium salts suggest a rather unspecific interaction. The salt ions may shield electrostatic repulsion between monomeric peptides with a net charge of −3 at neutral pH as well as act neutralizing of charges on the fibril surface. This charge effect on principal monomer-fibril interaction has been shown previously to affect

DOI: 10.1021/jacs.6b04511
J. Am. Chem. Soc. 2016, 138, 6893−6902

aggregation kinetics, where introducing charge−charge repulsion reduces formation of encounter complexes and consequently aggregation.[15] The shielding of electrostatic repulsion favors in particular secondary nucleation events, which have been characterized as the dominant nucleation mechanism.[9,11,16] This differs in comparison to the effect of zinc ions that has previously been shown to specifically interact with the Aβ40 peptide's N-terminus and interfere with the folding of the peptide at the fibril end and consequently reducing the fibril-end elongation rate, k_+, while leaving k_2 basically unaffected.[9] In addition to an effect on the nucleation process we found that (at least) two distinct fibril morphologies for Aβ40 fibrils can be detected, F_β and F_β*, where F_β seems to be energetically more stable under all studied conditions, but the barrier for the transition from the unfolded state, referred to as D, to the F_β state is dependent on salt and is significantly higher at low salt concentration. Hence F_β* is highly populated at short and intermediate time scales (Figure 6). In the presence of salt the free energy landscape seems to be less frustrated and the barrier is lower, leading to faster aggregation and direct formation of F_β. The fibril morphology may differ from each other in their tertiary and/or quaternary β-sheet arrangement, and can be characterized by their distinct CD signals, whereas, somewhat surprising, FTIR spectroscopy apparently is not sensitive for these different β-structures (see Supporting Information). These findings may contribute to an understanding and first order characterization of the free energy landscape of the numerous reported slightly different Aβ40 fibril structures obtained by solid-state nuclear magnetic resonance[37,50,51] and cryo-electron microscopy.[44,46,54]

Taken together, the findings obtained in this study provide insight in the molecular mechanism of Aβ40 aggregation and how it is modulated by ionic strength. In the presented model, screening of the electronic net charges promotes secondary nucleation reactions and favors the adoption of a low free energy state, F_β, in the β-structure morphology. This molecular framework might be beneficial for interpreting the polymorphism of amyloid fibril structures and understanding of protein misfolding pathways.

■ ASSOCIATED CONTENT

Supporting Information

The Supporting Information is available free of charge on the ACS Publications website at DOI: 10.1021/jacs.6b04511.

Additional figures, a table with all global fit parameters and a detailed discussion about FTIR-CD results. (PDF)

■ AUTHOR INFORMATION

Corresponding Author

*jens.danielsson@dbb.su.se

Present Address

§(A.A.): Department of Neurobiology, Care Sciences and Society, Center for Alzheimer Research, Division of Neurogeriatrics, Karolinska Institute, SE-141 86 Stockholm, Sweden.

Notes

The authors declare no competing financial interest.

■ ACKNOWLEDGMENTS

We acknowledge financial support by grants from the Swedish Research Council, the Swedish Brain Foundation, the Alzheimer Foundation, the Knut and Alice Wallenberg Foundation, the Magnus Bergwall Foundation and Estonian Ministry of Education and Research (IUT23−7).

■ REFERENCES

(1) Chiti, F.; Dobson, C. M. *Annu. Rev. Biochem.* **2006**, *75*, 333.
(2) Knowles, T. P.; Vendruscolo, M.; Dobson, C. M. *Nat. Rev. Mol. Cell Biol.* **2014**, *15*, 384.
(3) Haass, C.; Selkoe, D. J. *Nat. Rev. Mol. Cell Biol.* **2007**, *8*, 101.
(4) Cohen, S. I. A.; Vendruscolo, M.; Dobson, C. M.; Knowles, T. P. J. *J. Mol. Biol.* **2012**, *421*, 160.
(5) Wärmländer, S.; Tiiman, A.; Abelein, A.; Luo, J.; Jarvet, J.; Söderberg, K. L.; Danielsson, J.; Gräslund, A. *ChemBioChem* **2013**, *14*, 1692.
(6) Otzen, D. E. *Biophys. J.* **2002**, *83*, 2219.
(7) Klement, K.; Wieligmann, K.; Meinhardt, J.; Hortschansky, P.; Richter, W.; Fändrich, M. *J. Mol. Biol.* **2007**, *373*, 1321.
(8) Abelein, A.; Bolognesi, B.; Dobson, C. M.; Gräslund, A.; Lendel, C. *Biochemistry* **2012**, *51*, 126.
(9) Abelein, A.; Gräslund, A.; Danielsson, J. *Proc. Natl. Acad. Sci. U. S. A.* **2015**, *112*, 5407.
(10) Cohen, S. I. A.; Vendruscolo, M.; Welland, M. E.; Dobson, C. M.; Terentjev, E. M.; Knowles, T. P. J. *J. Chem. Phys.* **2011**, *135*, 065105.
(11) Meisl, G.; Yang, X.; Hellstrand, E.; Frohm, B.; Kirkegaard, J. B.; Cohen, S. I. A.; Dobson, C. M.; Linse, S.; Knowles, T. P. J. *Proc. Natl. Acad. Sci. U. S. A.* **2014**, *111*, 9384.
(12) Bulheller, B. M.; Hirst, J. D. *Bioinformatics* **2009**, *25*, 539.
(13) Hellstrand, E.; Boland, B.; Walsh, D. M.; Linse, S. *ACS Chem. Neurosci.* **2010**, *1*, 13.
(14) Szavits-Nossan, J.; Evans, M. R.; Majumdar, S. N. *Phys. Rev. Lett.* **2014**, *112*, 020602.
(15) Lang, L.; Kurnik, M.; Danielsson, J.; Oliveberg, M. *Proc. Natl. Acad. Sci. U. S. A.* **2012**, *109*, 17868.
(16) Cohen, S. I. A.; Linse, S.; Luheshi, L. M.; Hellstrand, E.; White, D. A.; Rajah, L.; Otzen, D. E.; Vendruscolo, M.; Dobson, C. M.; Knowles, T. P. J. *Proc. Natl. Acad. Sci. U. S. A.* **2013**, *110*, 9758.
(17) Ferrone, F. *Methods Enzymol.* **1999**, *309*, 256.
(18) Zhang, Y.; Cremer, P. S. *Curr. Opin. Chem. Biol.* **2006**, *10*, 658.
(19) Marek, P. J.; Patsalo, V.; Green, D. F.; Raleigh, D. P. *Biochemistry* **2012**, *51*, 8478.
(20) Baldwin, R. L. *Biophys. J.* **1996**, *71*, 2056.
(21) Kloss, E.; Barrick, D. *J. Mol. Biol.* **2008**, *383*, 1195.
(22) Lee, K. K.; Fitch, C. A.; Lecomte, J. T.; Garcia-Moreno, E. B. *Biochemistry* **2002**, *41*, 5656.
(23) Attard, P. *Adv. Chem. Phys.* **1996**, *92*, 1−159.
(24) Yoshiike, Y.; Tanemura, K.; Murayama, O.; Akagi, T.; Murayama, M.; Sato, S.; Sun, X.; Tanaka, N.; Takashima, A. *J. Biol. Chem.* **2001**, *276*, 32293.
(25) Tiiman, A.; Palumaa, P.; Tougu, V. *Neurochem. Int.* **2013**, *62*, 367.
(26) Roche, J.; Shen, Y.; Lee, J. H.; Ying, J.; Bax, A. *Biochemistry* **2016**, *55*, 762.
(27) Iesmantavicius, V.; Dogan, J.; Jemth, P.; Teilum, K.; Kjaergaard, M. *Angew. Chem., Int. Ed.* **2014**, *53*, 1548.
(28) Marsh, J. A.; Singh, V. K.; Jia, Z.; Forman-Kay, J. D. *Protein Sci.* **2006**, *15*, 2795.
(29) Arai, M.; Sugase, K.; Dyson, H. J.; Wright, P. E. *Proc. Natl. Acad. Sci. U. S. A.* **2015**, *112*, 9614.
(30) Fawzi, N. L.; Ying, J.; Torchia, D. A.; Clore, G. M. *J. Am. Chem. Soc.* **2010**, *132*, 9948.
(31) Fawzi, N. L.; Ying, J.; Ghirlando, R.; Torchia, D. A.; Clore, G. M. *Nature* **2011**, *480*, 268.
(32) Grüning, C. S.; Klinker, S.; Wolff, M.; Schneider, M.; Toksöz, K.; Klein, A. N.; Nagel-Steger, L.; Willbold, D.; Hoyer, W. *J. Biol. Chem.* **2013**, *288*, 37104.
(33) Sanchez, L.; Madurga, S.; Pukala, T.; Vilaseca, M.; Lopez-Iglesias, C.; Robinson, C. V.; Giralt, E.; Carulla, N. *J. Am. Chem. Soc.* **2011**, *133*, 6505.

DOI: 10.1021/jacs.6b04511
J. Am. Chem. Soc. 2016, 138, 6893−6902

(34) Narayan, P.; Orte, A.; Clarke, R. W.; Bolognesi, B.; Hook, S.; Ganzinger, K. A.; Meehan, S.; Wilson, M. R.; Dobson, C. M.; Klenerman, D. *Nat. Struct. Mol. Biol.* **2011**, *19*, 79.
(35) Barth, A. *Biochim. Biophys. Acta, Bioenerg.* **2007**, *1767*, 1073.
(36) Petkova, A. T.; Yau, W.; Tycko, R. *Biochemistry* **2006**, *45*, 498.
(37) Paravastu, A. K.; Leapman, R. D.; Yau, W. M.; Tycko, R. *Proc. Natl. Acad. Sci. U. S. A.* **2008**, *105*, 18349.
(38) Qiang, W.; Yau, W. M.; Luo, Y.; Mattson, M. P.; Tycko, R. *Proc. Natl. Acad. Sci. U. S. A.* **2012**, *109*, 4443.
(39) Lührs, T.; Ritter, C.; Adrian, M.; Riek-Loher, D.; Bohrmann, B.; Döbeli, H.; Schubert, D. a.; Roland, R. *Proc. Natl. Acad. Sci. U. S. A.* **2005**, *102*, 17342.
(40) Eisenberg, D.; Jucker, M. *Cell* **2012**, *148*, 1188.
(41) Fändrich, M. *Cell. Mol. Life Sci.* **2007**, *64*, 2066.
(42) Micsonai, A.; Wien, F.; Kernya, L.; Lee, Y. H.; Goto, Y.; Refregiers, M.; Kardos, J. *Proc. Natl. Acad. Sci. U. S. A.* **2015**, *112*, E3095.
(43) Manning, M. C.; Woody, R. W. *Biopolymers* **1987**, *26*, 1731.
(44) Sachse, C.; Xu, C.; Wieligmann, K.; Diekmann, S.; Grigorieff, N.; Fändrich, M. *J. Mol. Biol.* **2006**, *362*, 347.
(45) Petkova, A. T.; Leapman, R. D.; Guo, Z.; Yau, W. M.; Mattson, M. P.; Tycko, R. *Science* **2005**, *307*, 262.
(46) Meinhardt, J.; Sachse, C.; Hortschansky, P.; Grigorieff, N.; Fändrich, M. *J. Mol. Biol.* **2009**, *386*, 869.
(47) Bryngelson, J. D.; Wolynes, P. G. *Proc. Natl. Acad. Sci. U. S. A.* **1987**, *84*, 7524.
(48) Leopold, P. E.; Montal, M.; Onuchic, J. N. *Proc. Natl. Acad. Sci. U. S. A.* **1992**, *89*, 8721.
(49) Oliveberg, M. *Curr. Opin. Struct. Biol.* **2001**, *11*, 94.
(50) Petkova, A. T.; Ishii, Y.; Balbach, J. J.; Antzutkin, O. N.; Leapman, R. D.; Delaglio, F.; Tycko, R. *Proc. Natl. Acad. Sci. U. S. A.* **2002**, *99*, 16742.
(51) Bertini, I.; Gonnelli, L.; Luchinat, C.; Mao, J.; Nesi, A. *J. Am. Chem. Soc.* **2011**, *133*, 16013.
(52) Lu, J. X.; Qiang, W.; Yau, W. M.; Schwieters, C. D.; Meredith, S. C.; Tycko, R. *Cell* **2013**, *154*, 1257.
(53) Tiiman, A.; Jarvet, J.; Gräslund, A.; Vukojević, V. *Biochemistry* **2015**, *54*, 7203.
(54) Schmidt, M.; Sachse, C.; Richter, W.; Xu, C.; Fändrich, M.; Grigorieff, N. *Proc. Natl. Acad. Sci. U. S. A.* **2009**, *106*, 19813.

DOI: 10.1021/jacs.6b04511
J. Am. Chem. Soc. 2016, 138, 6893−6902